9 Phase transitions, new materials and superconducting γ-detectors

M. Reibelt, R. Dell'Amore, H. Bartolf, S. Siegrist, A. Engel and A. Schilling

in collaboration with:
Paul Scherrer Institute (Ch. Rüegg, J. Mesot, M. Medarde, K. Pomjakushina, K. Conder), University of Bern (K. Krämer), Bhaba Atomic Research Center (G. Ravikumar), Forschungszentrum Karlsruhe (Th. Wolf, H. Küpfer), Universität Karlsruhe (K. Il'in), ETH Zürich (J. Karpinski), Deutsches Zentrum für Luft- und Raumfahrt (H.-W. Hübers), University of Wellington (B. Ruck), Istituto Nazionale di Ricerca Metrologica I.N.RI.M Torino (C. Portesi), CSEM Neuenburg, FIRST Lab ETH Zürich.

Last year we have continued our activities at the FIRST Center for Micro- and Nanoscience at the ETH Zürich where we have successfully implemented a lift-off technique as an alternative to etching processes in the electron-beam lithography for producing superconducting thin-film photon detectors (H. Bartolf and A. Engel). We have also discovered a first-order like feature in the specific heat of a V_3Si single crystal near the transition to superconductivity, and studied the effect of the thermal and the magnetic history on this feature in detail. We have built a high-frequency susceptometer working in the MHz range which is necessary to study possible resonance phenomena in an exotic magnetic state of $TlCuCl_3$ (R. Dell'Amore). Finally we have continued our synthesis experiments on $LaSrNiO_4$ and related compounds to study the influence of cation and anion substitution on its electronic properties.

9.1 Physics of superconducting thin-film nanostructures and possible applications as fast single-photon detectors

The detectors we want to study and advance rely on the combined effect of quasi-particle multiplication upon absorption of a photon and a high bias current, which is just below the critical current of the superconducting meander. In a superconductor an absorbed photon leads to the break-up of a Cooper-pair. Because the photon energy is in general much larger than the superconducting gap energy a cascading process sets in during which many more Cooper-pairs are broken up resulting a cloud of quasi-particles. This cloud of quasi-particles at the absorption site is equivalent to a local reduction of the current-carrying capacity of the superconducting strip line. Eventually the bias current exceeds the local critical current and a voltage pulse is generated that can be registered with standard electronics. The main advantages of these detectors compared to other technologies is the ultra-high speed, the accuracy to determine the arrival time of a photon and the very high sensitivity.

E-beam lithography

In order to get a good detector it is of paramount importance that the complete device is as homogeneous as possible. Already very small variations in T_c, I_c or the cross-sectional area of the strip line lead to a reduced performance or even a complete failure. This implies great demands on the production process of the device. During the last year, we developed a three step lift-off process that enables us to generate nanometer-sized devices structured from

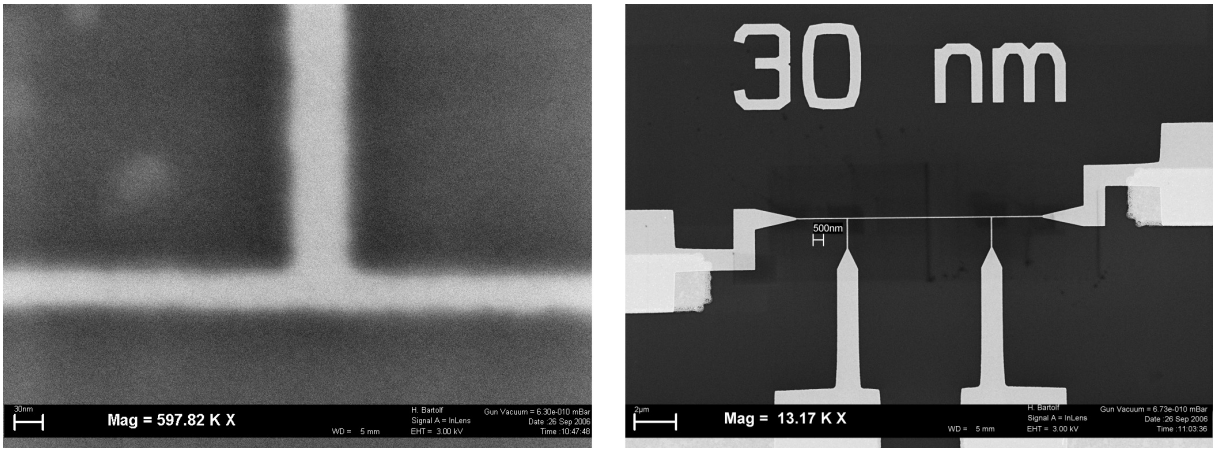

Figure 9.1: SEM pictures of a Au/Cr bridge with a width of 30 nm and thickness approximately 25 nm created with lift-off. The picture on the right shows the bridge and the connection pads that allow for 4-point resistance measurements. On the left we show a blow-up (rotated by 180°) of one of the voltage junctions at maximum resolution.

evaporated films, with thicknesses from only a few nanometers to some ten nanometers. The films are evaporated on a silicon substrate, and the layout is designed to allow for four point resistivity measurements on our devices. In the first step, bond pads, orientation marks (for the second optical lithography step and the third electron-beam lithographic step) are created by optical lithography, Cr/Au evaporation and a lift-off. We work with ma-N 405, a standard photolithographic resist, of 300 nm total thickness. The film thickness of the resulting structures is about 100 nm. In the second step connection pads are made by the same technique. The thickness of these pads is a fifth of that of the first structures, i.e. roughly 20 nm. Finally, electron-beam lithography and subsequent lift-off is used to define the nanostructures. In order to obtain very small feature sizes, we work with 1.6 nm step size, 30 kV acceleration voltage and a bilayer resist (PMMA 20 nm / copolymer 50 nm). Dose tests with thin resists show that we are able to achieve minimum feature sizes of about 10 nm (1). In Fig. 9.1 we show a SEM picture of a 30 nm wide bridge fabricated with the above described process. This bridge is made of approximately 25 nm thick Au on top of a roughly 1 nm thick Cr adhesion layer. For ease of use and to demonstrate the feasibility of our process most structures produced so far are made of similar Au films. In a next step we plan to use superconducting films.

Transition metal nitrides

Currently, NbN is used as the standard material for these kind of single-photon detectors. In many respects NbN is a very good material, not only because of its favorable superconducting properties, but also because it is well characterized and there is considerable experimental experience with it. However, it has a relatively high critical temperature limiting its useful spectral range to visible and near-infrared radiation. This is our motivation to explore other superconducting materials as possible alternatives to NbN. In 2006 we started to look at other transition metal nitrides. With the exception of Cr all neighboring elements to Nb in the periodic table also form superconducting nitrides with T_c values of several Kelvin. In a first attempt we tried to grow TaN films. Ta was evaporated by means of an e-gun in a N_2 atmosphere at about 9×10^{-5} mbar and a small flux of

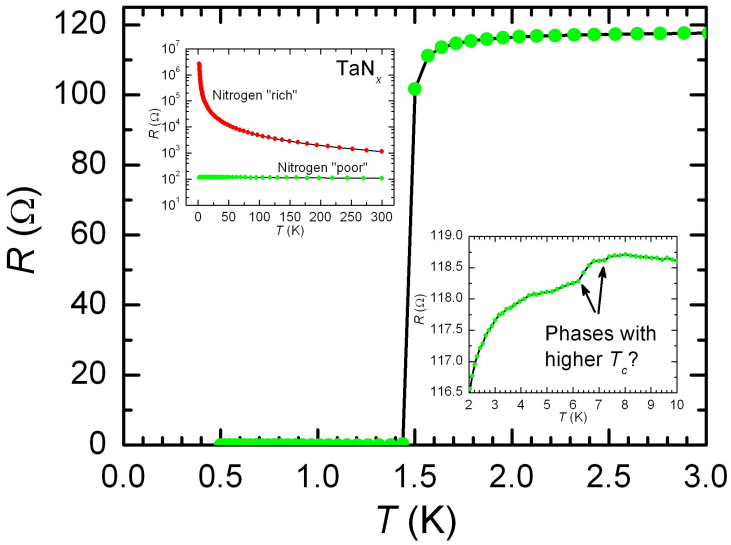

Figure 9.2: The upper left inset shows resistance v.s. temperature data for two TaN films with low and high N-content as indicated. As shown in the main graph the film with a reduced N-content becomes superconducting at $T_c \approx 1.45$ K. The blow-up of the temperature range from 2 to 10 K in the lower right inset reveals steps in the resistance data, which we attribute to superconducting transitions of small inclusions with higher T_c.

N_2^+-ions. Ta and N form various stable phases with different N-content. Adjusting the current density due to the flux of N_2-ions we could tailor the characteristics of the resulting films from semiconductor-like for those films with a high N-content to metallic for films with a reduced amount of N. To prevent oxidation, films with a reduced N-content were protected by a GaN capping layer. The films were deposited onto sapphire and Si substrates held at constant temperatures during evaporation ranging from $80°$C to about $120°$C. Based on previous experience with Ta evaporation in the same vacuum chamber, we expected highly disordered or even amorphous films.

This expectation was confirmed by x-ray analysis, which showed no sign of crystalline structure, and the temperature dependence of the resistance. In the upper left inset of Fig. 9.2 we show resistance data for two films from room temperature down to below 10 K. The nitrogen-rich film exhibits a clearly non-metallic behavior, whereas the nitrogen-poor has a small negative temperature coefficient, typical for strongly disordered or amorphous metals. The latter film does become superconducting at a $T_c \approx 1.45$ K, see the main graph of Fig. 9.2; considerably lower than for bulk crystalline TaN with a $T_c = 14$ K, but still higher than for amorphous Ta ($T_c = 0.9$ K). In the lower right inset of Fig. 9.2 we show a blow-up of the resistance data of the metallic TaN film between 2 and 10 K. Here we observe several small steps in the resistance curve. These steps shift and eventually vanish when we increased the measuring current. We interpret these steps as signs of small inclusions in our films with higher T_c. With further optimization of deposition parameters and additional annealing of the films at higher temperatures, we are hopeful to increase T_c into a range where the films might become useful for detector applications.

T-dependence of the critical current

One of the key operating parameters of the single-photon detectors is the bias current, which is adjusted to about 90% to 95% of the critical current. The ratio between bias current and critical current directly influences the sensitivity of the detectors. In addition there may be more subtle effects related to the absolute value of the bias current, e.g. caused by the interaction between bias current and vortices, which could be present in the strip line. Knowledge of the temperature-dependence of the critical current of the strip line is therefore necessary to choose the best possible

operating conditions. Within standard GL-theory one expects a smooth and continuous increase of the critical current with decreasing temperature. Preliminary measurements of the critical current on NbN bridges with widths ranging from 10 μm down to 300 nm showed various unexpected kinks and sometimes even steps in their temperature dependence. We have now started to systematically investigate these effects.

9.2 A history dependent first-order like phase transition feature near H_{c2} in V_3Si

V_3Si and Nb_3Sn share the same cubic "β-tungsten (A-15)" structure. Nb_3Sn is frequently used in technical applications, therefore the phase diagram of this class of materials is not only of academic interest. Besides the superconducting transition at the H_{c2}-line the rich phase diagram of V_3Si also features an irreversibility line, a peak-effect region, a low-field and a high-field phase-transition line which separates a quasi-ordered Bragg glass phase from a disordered phase of the vortex matter, a flux-line lattice reorientation line between a hexagonal and cubic symmetry, and in most crystals a structural phase transition can also be observed.

A15 compounds such as Nb_3Sn and V_3Si are well known to exhibit such a structural transition from a high-temperature cubic to a low-temperature tetragonal phase. This transformation is often called "martensitic transition" and is believed to be driven by a Peierls instability. Its origin is a band-type Jahn-Teller effect which leads to the formation of a Peierls like energy gap (2). Several experimental and theoretical studies (3; 4) have been carried out to clarify a correlation between the martensitic transition (in general the lattice instability) and the relatively high T_c in these conventional superconductors, because the A15 compounds showed the highest known T_c before the discovery of the high-T_c materials by Müller and Bednorz in 1986. It was found that the structural transition affects the superconducting transition in various ways which leads to a net decrease of the transition temperature T_c by approximately 0.3 K in the tetragonal phase. Superconductivity has, in turn, a more profound effect on the martensitic transition. It was predicted by theoretical models and also found in experiments that the developing tetragonality upon cooling is interrupted at the transition to superconductivity. If the superconducting transition occurs already in the cubic phase, the martensitic transition is completely suppressed and the crystal remains cubic.

We have observed a so far unreported first-order like phase transition feature in the specific heat of a single crystalline sphere of V_3Si that depends on the thermal history of the sample and that occurs very close to the H_{c2} line. The martensitic transition is very close to the transition to superconductivity in our crystal, and we assume that this proximity to H_{c2} is relevant for the occurrence of the observed effect.

Fig. 9.3 shows the specific heat of the V_3Si sample ($m = 11.1$ mg) measured in a commer-

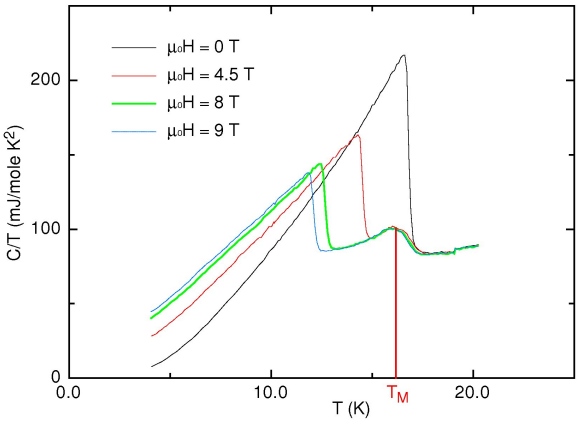

Figure 9.3: Specific heat of a V_3Si single crystal measured in a commercial PPMS by a conventional heat relaxation technique. The superconducting and the martensitic transition are clearly observable, but no first-order like peak can be resolved near H_{c2}.

cial PPMS system (Quantum Design) by a conventional heat-relaxation technique. Both the superconducting and the martensitic transitions are observable as continuous phase transitions. The estimated transition width ΔT_c from these data for $\mu_0 H = 0$ T is $\Delta T_c = 280$ mK, and the specific-heat discontinuity at T_c in zero field is $\Delta C/T = 143$ mJ/mol K^2. In zero magnetic field the martensitic transition (at T_M) is suppressed by the superconducting state. Since T_M decreases much less than the critical temperature T_c with increasing magnetic field, the martensitic transition is fully developed for $\mu_0 H = 1$ T (for lower magnetic fields only the onset of the martensitic transition is observable). No first-order like peak can be resolved near T_c in this type of experimental set up.

We have investigated the same sample with a DTA (differential-thermal analysis) method that is particularly well suited for the detection of sharp phase transitions in samples of milligram size (5; 6). We collected data in 18 different magnetic fields parallel to the $[100]$ direction of the crystal. In Fig. 9.4 we show some of these results (data for intermediate fields are not shown for clarity reasons), scaled with the PPMS data from Fig. 9.3. The estimated transition width ΔT_c for $\mu_0 H = 0$ T is only $\Delta T_c = 75$ mK, which is considerably less than the corresponding value obtained from the PPMS data. Our DTA method is indeed able to measure variations in entropy without being affected by any instrumental broadening of the data, in contrast to conventional methods to measure a specific heat, including the relaxation method used by the PPMS (5; 6).

Surprisingly, for all magnetic fields above $\mu_0 H = 1$ T a distinct first-order like peak can be resolved at a temperature T_p near T_c with a width of approximately $\Delta T_p = 36$ mK. Fig. 9.5 shows DTA data for $\mu_0 H = 7$ T on an expanded scale, and we have marked the relevant temperatures that we have used to draw the phase diagram shown in Fig. 9.6.

The absence of this sharp feature in corresponding literature data may be explained by a lower data-point density and/or a certain instrumental broadening of such data. Another possibility may be the fact that the occurrence of the observed feature turned out to strongly depend on the cooling history of the sample. The peak appears only for a fast cooling rate (i.e., of the order of 200 mK/sec) prior to a measurement, and disappears for a very slow cooling rate (0.2 mK/sec, data not shown).

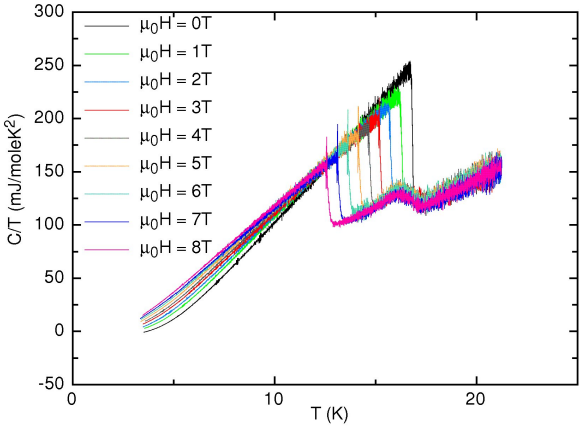

Figure 9.4: Field dependence of the specific heat measured in a DTA-cell and for magnetic fields parallel [100]. A first-order like peak appears for fields μ_0H≥1 T close to T_c.

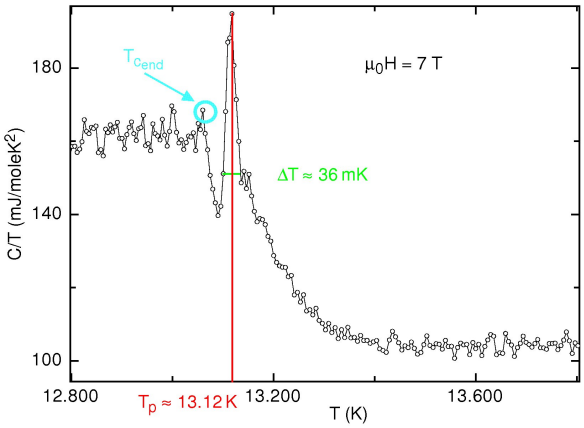

Figure 9.5: Representative specific-heat measurement for μ_0H = 7 T on an expanded scale.

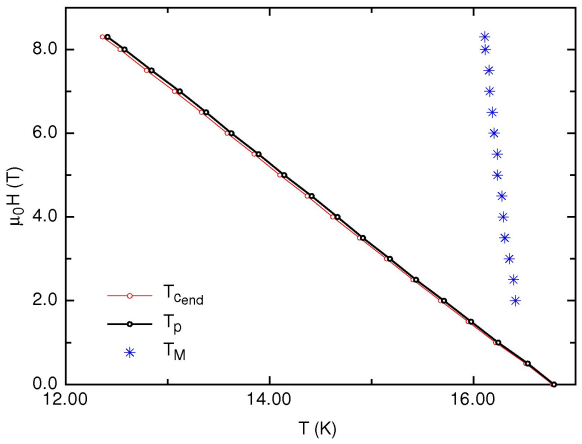

Figure 9.6: Phase diagram of the investigated V_3Si single crystal. T_c and T_p (see Fig. 9.5) are very close to each other, while T_M is almost field independent.

Interestingly the feature does not depend on the magnetic history, e.g., cooling in the magnetic field (FC) or zero-field cooling (ZFC). The use of external coils that produce a transverse ac "shaking" field also did not show any effect on the observed phenomenon. These facts, together with the observation that the entropy change associated with the first-order like peak does not scale with the external magnetic field, indicate that the peak in C/T is probably not related to a transition of vortex lattice. This conclusion is supported by the peculiar strong angular dependence of the feature when the magnetic field is rotated away from the $[100]$ direction, and by the results from SQUID magnetization measurements (by S. Weyeneth, group of Prof. Keller) that do not show any clear signature at the corresponding temperatures as we may expect for a vortex-related phase transition.

9.3 Search for resonance phenomena in $TlCuCl_3$ in the MHz range

Low dimensional quantum spin systems exhibit a variety of quantum phenomena that have gained much in interest in the last decade (7; 8; 9; 10). Our work is focused on $\mathrm{TlCuCl_3}$ for two particular reasons. This material was one of the first solids, in which experimental work indicated that the magnetic quasiparticles (magnons) form a Bose-Einstein condensate (BEC) above a critical field $\mu_0 H_c \approx 5.5\mathrm{T}$ at low temperatures (8; 11). Meanwhile several other materials have been found, that exhibit various features which can be explained within the framework of a condensation of quasiparticles with integer spin (9; 10; 12). Limitations of our cryo-system (such as the lowest reachable temperature and the highest applicable magnetic field) do not allow us to investigate this phenomenon in other materials than $\mathrm{TlCuCl_3}$, however.

The discovery of a BEC-like scenario of different types of quasiparticles in all these different materials raised various questions (13). In one case (14), the lifetime of the quasiparticles is very short (a few picoseconds). In other cases the number of quasiparticles is not conserved (15) or symmetry aspects are not entirely fulfilled (16). To what extent these unfavorable conditions affect the Bose-Einstein condensation is still an issue of debate. To prove that there is in fact a true condensate one has to show that the particles form a single coherent state, similar to the superfluid state as observed in liquid $^4\mathrm{He}$. A convincing method would therefore be to demonstrate the existence of such a superfluid component in the system. In analogy to $^4\mathrm{He}$, a second-sound mode in such a condensate phase would manifest itself as an oscillation of the density of the quasiparticles (superfluid and normalfluid component flow relative to one another) and accordingly of the entropy in the system. The detection of such a mode would therefore be a clear sign for the occurrence of a BEC.

Last year we have performed our measurements on $\mathrm{TlCuCl_3}$ at $\mathrm{T} = 2\mathrm{K}$ and $\mu_0\mathrm{H} = 9\mathrm{T}$ with a home-made AC driven Wheatstone-like bridge set-up. However, the resulting data have not revealed the distinct resonances that we have expected to occur due to

a "second-sound mode" of a possible BEC-state. The occurrence of many sharp resonances in the background signal made the detection of the expected small signals coming from the sample quite unreliable. Performing an immediate background subtraction, moving the sample in and out of the detection coil "in situ" in helium atmosphere has not resulted in a significant improvement. Therefore we decided to design a new detection coil set-up, in which no current is flowing through the coils in order to avoid undesired resonance phenomena resulting in a relatively large and arbitrary background signal.

We built a new AC susceptometer to perform high-frequency magnetic-susceptibility measurements from 200 kHz up to 2 MHz. The design is a standard 3-coil configuration with a primary coil and two secondary pick-up coils (see Fig. 9.7). A highly symmetric arrangement of the secondary coils with respect to each other and their immediate surroundings is necessary to avoid any unbalance of the induced voltage signal. Imperfections of the two pick-up coils or just a slight inhomogeneity of the AC magnetic field in the primary coil cause a non-zero induced voltage even in absence of any sample (see Fig. 9.8). A step motor enables us to move the sample in and out of the pick-up coils, or to move it from one secondary coil to the other one. Thus an immediate background subtraction is implemented. Any residual offset strongly increases with measuring frequency and amplitude of the AC magnetic field, however.

The impedance of the primary coil with inductance L, $Z = i\omega L$, also increases with frequency, which results in a limitation of the current passing through the coil and consequently of the amplitude of the generated AC magnetic field. A powerful high-frequency current source was therefore designed and built in collaboration with our domestic electronic work-shop. As a signal analyzer we use a standard lock-in amplifier (EG & G Instruments 7260 DSP lock-in amplifier) or a spectrum analyzer (Rohde & Schwarz FSL spectrum analyzer), which enables us to perform a larger frequency scan in a shorter time period limiting the resolution bandwidth to 10 Hz (every measured data point is averaged over 10 Hz). First measurements with this new set-up still revealed an insufficient sensitivity over the large studied frequency range due to remaining unbalance of the signal. Therefore an even more precise voltage compensation circuit is required, which is still under construction.

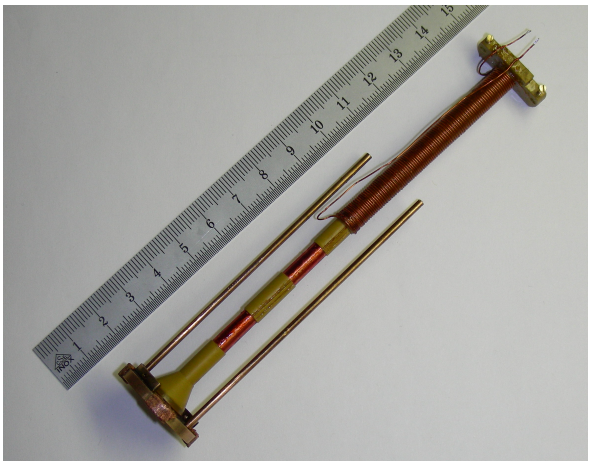

Figure 9.7: The disassembled coil system for measuring high-frequency AC susceptibility, showing both primary coil and the secondary pick-up coils.

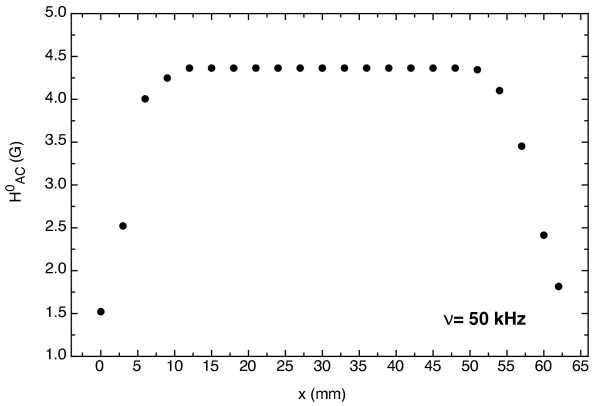

Figure 9.8: Magnetic-field profile of the primary coil.

9.4 Cation and anion substitution in $LaSrNiO_4$ and $LaBaNiO_{4-\delta}$

Last year we had reported that polycrystalline $LaBaNiO_{4-\delta}$ samples as-prepared by standard wet chemical procedures) are oxygen deficient ($\delta = 0.15$), which might explain the poor electrical conductivity as compared to metallic $LaSrNiO_4$, because also the planar oxygen atoms seem to be affected. We have hypothesized that fully oxygenated $LaBaNiO_{4-\delta}$ might behave in a very different way as soon as $\delta = 0$ is achieved. To verify this hypothesis we have prepared single phased $LaBaNiO_{4-\delta}$ and $LaSr_{0.5}Ba_{0.5}NiO_4$, and annealed the samples at $400°C$ at an O_2 pressure of 880 bar (in collaboration with J. Karpinksi, ETHZ).

Chemical analysis (done by K. Pomjakushina, LNS) revealed an oxygen content $4.03(1)$ confirming the desired oxygen stoichiometry. In Fig. 9.9 we show the electrical conductivity in comparison with corresponding data from metallic $LaSrNiO_4$. The electrical conductivity of $LaBaNiO_4$ still shows a pronounced variable-range hopping-type temperature dependence over a wide range of temperatures. Therefore it is clear that the electrical transport in $LaBaNiO_4$ is indeed intrinsically different from that in $LaSrNiO_4$.

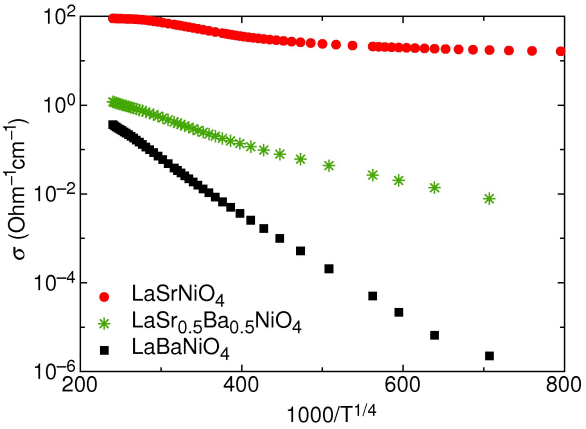

Figure 9.9: Electrical conductivity of $LaSrNiO_4$, $LaSr_{0.5}Ba_{0.5}NiO_4$, and $LaBaNiO_4$ after high oxygen-pressure annealing. $LaBaNiO_4$ exhibits an almost perfect variable-range hopping-type conductivity.

In an attempt to modify the physical properties of $LaSrNiO_4$ we made a number of substitution experiments, e.g., by replacing La or Sr with elements of smaller ionic radii, i.e., by the application of "chemical pressure". Up to now, only the stoichiometric compounds $RESrNiO_4$ with RE = La, Nd, Sm, Eu, and Gd have been reported to exist (all metallic) (17), while partial substitution has been achieved for $Dy_{1.5}Sr_{0.5}NiO_4$ (18), and $Nd_{1.4}Ca_{0.6}NiO_4$ (19). Our preparation under elevated oxygen pressure (1 kbar at $1000°C$) resulted in the formation of the new compounds $DySrNiO_4$, $HoSrNiO_4$, $NdCaNiO_4$ and $SmCaNiO_4$ (at present, no structural refinement has been made to ensure the exact cation stoichiometry).

Finally, a number of attempts have been made to change the electronic structure of $LaSrNiO_4$ by replacing the apical oxygen in the oxygen octahedra by halogen atoms. This substitution has been reported to be possible in transition-metal perovskites with the K_2NiF_4 structure for the case of Cu (substitution with F, Cl or Br (20; 21)), Fe (Cl or Br (22)), Co (Cl or Br (23)), and Mn (Cl (24)). In analogy to these structures we might expect the existence of compounds such as Sr_2NiO_3X or Ca_2NiO_3X with X = F, Cl or Br. Among the several possible synthesis techniques described in the literature we chose to fluorinate with NH_4F and to try a direct solid-state reaction using $NiCl_2$. In none of these experiments any compounds with the K_2NiF_4 structure and containing halogen atoms were formed.

[1] H. Bartolf, et al.,
in *Electron beam applications at ETH Zürich*, Raith Application Note 2006, Raith GmbH.

[2] G. Bilbro and W. L. McMillan,

Phys. Rev. B **14**, 1887 (1976).
[3] N. Toyota, T. Kobayashi et al., J. Phys. Soc. Jap. **57**, pp. 2089-3101 (1988).
[4] L. R. Testardi: Rev. Mod. Phys. **47**, 637 (1975).
[5] A. Schilling and O. Jeandupeux, Phys. Rev. B **52**, 9714 (1995).
[6] A. Schilling and M. Reibelt, Rev. Sci. Instrum. **78**, 033904 (2007).
[7] B.C. Watson et al., Phys. Rev. Lett. **86**, 5168 (2001).
[8] Ch. Rüegg et al., Nature **423**, 62 (2003).
[9] B. Grenier et al., Phys. Rev. Lett. **92**, 087203 (2004).
[10] V.S. Zapf et al., Phys. Rev. Lett. **96**, 077204 (2006).
[11] T. Nikuni et al., Phys.Rev. Lett. **84**, 5868 (2000).
[12] M. Jaime et al., Phys. Rev. Lett. **93**, 077204 (2004).
[13] D. Snoke et al., Nature **443**, 403 (2006).
[14] J. Kasparzak et al., Nature **443**, 409 (2006).
[15] S.O. Demokritov et al., Nature **443**, 430 (2006).
[16] V.N. Glazkov et al., Phys. Rev. B **69**, 184410 (2004).
[17] G. Demazeau et al., J. Solid State Chem. **18** (1976) 159, M. James and J. P. Attfield, J. Mater. Chem. **6** (1996) 57.
[18] G. L. Lu et al., Hua Hsueh Hsueh Pao **54** (1996) 667.
[19] Y. Takeda, et al., J. Solid State Chem. **96** (1992) 72.
[20] M. Al-Mamouri et al., Nature **369** (1994) 382.
[21] B. Grande and H. Müller-Buschbaum, Z. Anorgan. Allg. Chem. **429** (1977) 88.
[22] J. A. Ackerman, J. Solid State Chem. **92** (1991) 496.
[23] C. S. Knee and M. T. Weller, J. Solid State Chem. **168** (2004) 1.
[24] C. S. Knee and M. T. Weller, Chem. Commun. **3** (2002) 256.